# Preparation of carbon fiber cloth supported porous CdS nanorods with excellent photocatalytic activity for Cr(Ⅵ) reduction

LI Hengchao[1a], WANG Wenguang[1a*], WU Liangpeng[2], JIAN Siyuan[1a], LONG Shimin[1a], GUO Yuxi[1b]
(1 Guangdong University of Technology, a. School of Materials and Energy; b. School of Chemical Engineering and Light Industry, Guangzhou 510006, China; 2 Advanced Energy Science and Technology Guangdong Laboratory, Huizhou 516000, Guangdong China)

**Abstract** The use of visible-light responsive photocatalysts for removing heavy metal ions in wastewater has received great attention. However, the development of photocatalysts with high activity and recyclability remains a huge challenge. Herein, a recyclable carbon fiber cloth-supported porous CdS nanorod photocatalyst was fabricated by a two-step hydrothermal treatment using $AgVO_3$ nanowires as templates. The results indicated that under visible-light illumination, the carbon cloth-supported porous CdS nanorods showed improved photocatalytic activity for the reduction of Cr(Ⅵ), with an apparent rate constant exceeding that of carbon cloth-supported CdS nanospheres by a factor of 1.65 times. Moreover, the carbon cloth-supported porous CdS nanorods can be easily separated and be reused. This brings a new perspective for developing photocatalysts with high efficiency and recyclability for wastewater treatment.

**Keywords** carbon cloth; cadmium sulfide; silver metavanadate; porous nanorods; heavy metal ions reduction
**中图分类号** TB34 **文献标志码** A **文章编号** 1672-4321(2025)01-0009-13
**doi**:10.20056/j.cnki.ZNMDZK.20250744

# 碳布负载多孔CdS纳米棒光催化剂的制备及其高效Cr(Ⅵ)还原光催化活性

李恒超[1a], 王文广[1a*], 吴梁鹏[2], 简思源[1a], 龙诗敏[1a], 郭禹希[1b]
(1 广东工业大学 a.材料与能源学院; b.轻工化工学院, 广州 510006;2 先进能源科学与技术广东省实验室, 广东 惠州 516000)

**摘 要** 利用可见光响应光催化剂去除废水中重金属离子的技术已受到广泛关注.然而,开发具有高光催化活性和易回收利用的光催化材料仍然是一个挑战.以$AgVO_3$纳米线为模板,采用两步水热法制备了易回收的碳布负载多孔CdS纳米棒光催化剂.结果表明:在可见光照射下,碳布负载多孔CdS纳米棒对Cr(Ⅵ)表现出增强的光催化还原活性,其表观速率常数是直接在碳布上负载的CdS纳米球的1.65倍.此外,碳布负载多孔CdS纳米棒易于分离和重复使用,这为开发高效和可循环利用的光催化剂并应用于处理废水提供了新的思路.

**关键词** 碳布;硫化镉;偏钒酸银;多孔纳米棒;重金属离子还原

Industrial wastewater discharged from electroplating, chemical, printing and dyeing, and tanning industries usually contains a large amount of hexavalent chromium (Cr(Ⅵ)). Long-term exposure to hexavalent chromium will cause damage to human kidneys and liver, leading to emesis, diarrhea and other symptoms even cancer risk[1]. In comparison to Cr(Ⅵ), trivalent chromium (Cr(Ⅲ)) is generally non-toxic and can be safely

**收稿日期** 2024-03-05
* **通信作者** 王文广(1982-),男,副教授,博士,研究方向:光催化材料,E-mail: wwg2014@gdut.edu.cn
**基金项目** 国家自然科学基金资助项目(52072079,52202222,51802305);广东省自然科学基金资助项目(2021A1515010445)

absorbed by humans and animals as a trace element. Therefore, the reduction of Cr(Ⅵ) to Cr(Ⅲ) is one of the effective ways to deal with the pollution of Cr(Ⅵ) as heavy metal ion. The traditional ways for removing Cr (Ⅵ) contain chemical reduction method and electrolytic reduction method followed by chemical precipitation process[2-3]. However, these treating processes are always complicated with high cost accompanied by adjusting pH all the time. Since Jeon attempted to probe into the impact of $Nb_2O_5$ in $TiO_2$ on the reduction of $K_2Cr_2O_7$ under Xenon lamp illumination[4], photocatalytic technology has been preferably applied as a hopeful route for the reduction of Cr (Ⅵ) to harmfulless Cr (Ⅲ) in wastewater treatment [5-7].

In recent years, a variety of photocatalysts have been explored for removing Cr(Ⅵ), such as $TiO_2$[8], ZnO[6, 9], CdS[10-11], $Ag_2O$[12], $SnS_2$[13], metal-organic framework materials[7, 14], etc. Among them, cadmium sulfide (CdS) with a narrow band gap has sparked much attention due to its excellent properties including broad-spectrum visible-light absorption[15-16], good carrier transportation capacity and higher conduction band potential than the $H^+/H_2$ redox potential, which is widely used in the field of photocatalytic hydrogen production[17-21]. Currently, CdS with various morphologies such as nanoparticles, spheres, nanowires and nanorods have been prepared[22-25]. However, most of the CdS nanorods that had been reported are solid with small specific surface area[26]. The preparation of porous CdS nanorods with large specific surface area is still a challenge. Meanwhile, the powdered photocatalysts exhibit some disadvantages such as difficult recycling and secondary pollution in the practical application. Therefore, extensive research work has been undertaken to develop photocatalysts with large area, high photocatalytic activity and easy recycling[27].

Carbon fiber cloth has broad prospects due to its special properties such as excellent pliability, excellent electrical conductivity, high mechanical intensity and good resistant to corrosion, which has been broadly applied to be a substrate for *in situ* growth of nanomaterials that are applicable to photocatalysts, fuel cells, supercapacitors and lithium batteries[28-31]. Our group had prepared $MoS_2/Ag_2S/Ag_3PO_4$ composite on carbon fiber cloth which exhibited good photocatalytic activity and recyclability for photodegradation of rhodamine B[32]. Template-based method is a simple and controllable means to synthesize unique structures of nanomaterials[33]. In this work, we successfully synthesized carbon cloth-supported porous CdS nanorods using $AgVO_3$ nanowires as templates by a two-step hydrothermal method[34-35]. As for all we know, there were no studies reporting the preparation of porous CdS nanorods loaded on carbon fiber cloth. The carbon cloth-supported porous CdS nanorods exhibited an excellent photocatalytic reducibility to Cr (Ⅵ) when irradiated with visible light. And the CdS-loaded carbon cloth can be readily extracted from the solution system and be reused without loss in weight. The work may provide a way to design various kinds of recyclable photocatalysts that can be produced in large amounts and be used to purify wastewater containing heavy metal ions.

## 1 Materials and methods

### 1.1 Pretreatment of carbon cloth

A piece of square carbon cloth with size of 2 cm × 2 cm (WOS: 1009-17070602, average thickness: 0.33 mm, nominal basic weight: 115.0 $g \cdot m^{-2}$) was ultrasonic rinsed sequentially with acetone, ethanol, and deionized water to wipe off surface stains. Whereafter, the clean carbon cloth was dipped in nitric acid (65%) solution for 24 h to obtain good hydrophilic surface. After three times of rinse with deionized water, it was put into an oven keeping at 70 ℃ for drying.

### 1.2 Preparation of carbon cloth-supported $AgVO_3$ nanowires

$AgVO_3$ nanowires were created on the periphery of carbon fiber cloth via the hydrothermal method. Firstly, 12.36 mmol of $AgNO_3$ was added into 15 mL of deionized water to make it fully dissolved and form a colorless and transparent solution A. Meanwhile, 5.98 mmol of silver metavanadate ($NH_4VO_3$) and 24.98 mmol of urea ($CO(NH_2)_2$) were dissolved in

25 mL of nitric acid ($HNO_3$, 2 mol·$L^{-1}$) to form a homo-transparent solution B. Secondly, the pretreated carbon cloth was immersed in solution A for 6 h and then transferred to solution B soaking for 1 min. After that, the carbon cloth was transferred to solution A again for 1 min and soaked in solution B for 1 min once more. The to-and-fro soaking process was repeated for 20 times to ensure full adsorption of the precursors. Thirdly, the solution B was incorporated into the solution A and the obtained mixed solution was magnetic stirred for 10 min, followed by being poured into a hydrothermal reactor. Afterwards, the carbon cloth was placed vertically into the reactor, which was then removed into a drying oven and heated to 180 ℃ for 18 h. After the reactor dropped to the same temperature as the surroundings, the carbon cloth-supported $AgVO_3$ (denoted as CC/$AgVO_3$) was moved away from the reactor and cleaned with deionized water as well as ethanol for three times, and finally dried at 70 ℃ for 5 h.

### 1.3 Preparation of carbon cloth-supported porous CdS nanorods

The carbon cloth-supported porous CdS nanorods were prepared by combining template method with hydrothermal reaction. Specifically, 4.99 mmol of cadmium chloride ($CdCl_2·2.5H_2O$), 29.9 mmol of thiourea ($CH_4N_2S$) and 0.49 g of polyethylene glycol were dissolved into 40 mL of deionized water and a milk-white solution was taking form, which was then poured into a Teflon container with stainless-steel as outer lining. Subsequently, the CC/$AgVO_3$ was placed vertically into the reactor and heated up to 140 ℃ for 15 h. After the reactor cooled down to ambient temperature, the obtained carbon cloth-supported porous CdS nanorods (denoted as CC/P-CdS) was taken out and washed with deionized water and ethanol for several times, and finally heated up to 70 ℃ for 5 h in the drying oven. For comparison, the carbon cloth-supported CdS (denoted as CC/CdS) was also prepared by the same method using pretreated pure carbon cloth instead of CC/$AgVO_3$.

### 1.4 Characterization

The phase constitution and crystalline structure of the samples were studied by a X-ray diffractometer (XRD, D/MAX-Ultima Ⅳ, Rigaku, Japan) using Cu Kα radiation and the scanning rate was 8°·$min^{-1}$. The microstructure observation of the carbon cloth-supported photocatalysts was carried out on a field emission scanning electron microscope (FESEM, SU8010, Hitachi, Japan) and a transmission electron microscope (TEM, JEM2010F, JEOL, Japan). X-ray photoelectron spectroscopy (XPS) was measured on an X-ray photoelectron spectrometer (Thermo Fisher, Thermo Scientific K-Alpha, Waltham, USA) excited by Al Kα radiation. UV-Vis diffuse reflectance spectra (DRS) of the samples were tested on an UV-Vis spectrophotometer (Metash, UV9000, Shanghai, China) using $BaSO_4$ as a standard reflectance sample.

### 1.5 Photocatalytic activity test

The photocatalytic activity of the carbon cloth-supported photocatalysts was appraised by reducing the Cr (Ⅵ) ions in $K_2Cr_2O_7$ solution at ambient temperature. An LED lamp was used as the optical source and the wavelength was fixed to be 420 nm. Concretely speaking, a slice of carbon cloth loaded with the photocatalyst was placed vertically in a beaker holding 60 mL of $K_2Cr_2O_7$ solution. The entire mixture was put in the dark and magnetic stirred for 1 h to achieve an adsorption-desorption equilibrium before turning on the light. The amount of Cr (Ⅵ) was measured using the diphenylcarbazide colorimetric method and the absorption of light by solution was estimated using the UV-Vis spectrophotometer. The wavelength of the characteristic absorption peak is 540 nm. The photocatalytic performances of the catalysts were estimated by comparing the apparent reaction rate constant $k$ ($k$=In($C_0$/$C_t$)/$t$), where $C_0$ and $C_t$ are the concentrations of $K_2Cr_2O_7$ at adsorption equilibrium (before turning on the light) and at irradiation time $t$, respectively.

### 1.6 Computational-DFT calculation

The first-principle calculations were accomplished using the density-functional theory (DFT) method on the Materials Studio software with Cambridge Sequential Total Energy Package (CASTEP) code [36]. The calculation of geometric optimization was performed using the Perdew-Burke-Ernzerhof (PBE) approximation in generalized gradient approximation

(GGA). The electrical characteristics including states density and band structure were generated by hybrid functions of Heyd-Scuseria-Ernzerhof (HSE06). The geometry optimization of all the models was conducted based on the Broyden-Fletcher-Goldfarb-Shannon (BFGS) algorithm. The selected cutoff energy was 350 eV, and the k-point of the Brillouin zone was 4 × 4 × 4, as shown in Fig. 1. The ion nucleus was described using an ultrasoft pseudopotential. The pseudopotential was used and the valence electron configurations of the cadmium (Cd) and sulfur (S) atoms were $4d^{10}$ $5s^2$ and $3s^2$ $3p^4$, respectively. The convergence criteria for the total energy, the SCF energy, the maximum force, stress and displacement were set as $2\times10^{-5}$ eV·atom$^{-1}$, $2\times10^{-6}$ eV·atom$^{-1}$, 0.05 eV·Å$^{-1}$, 0.05 GPa and $1\times10^{-3}$ Å, respectively.

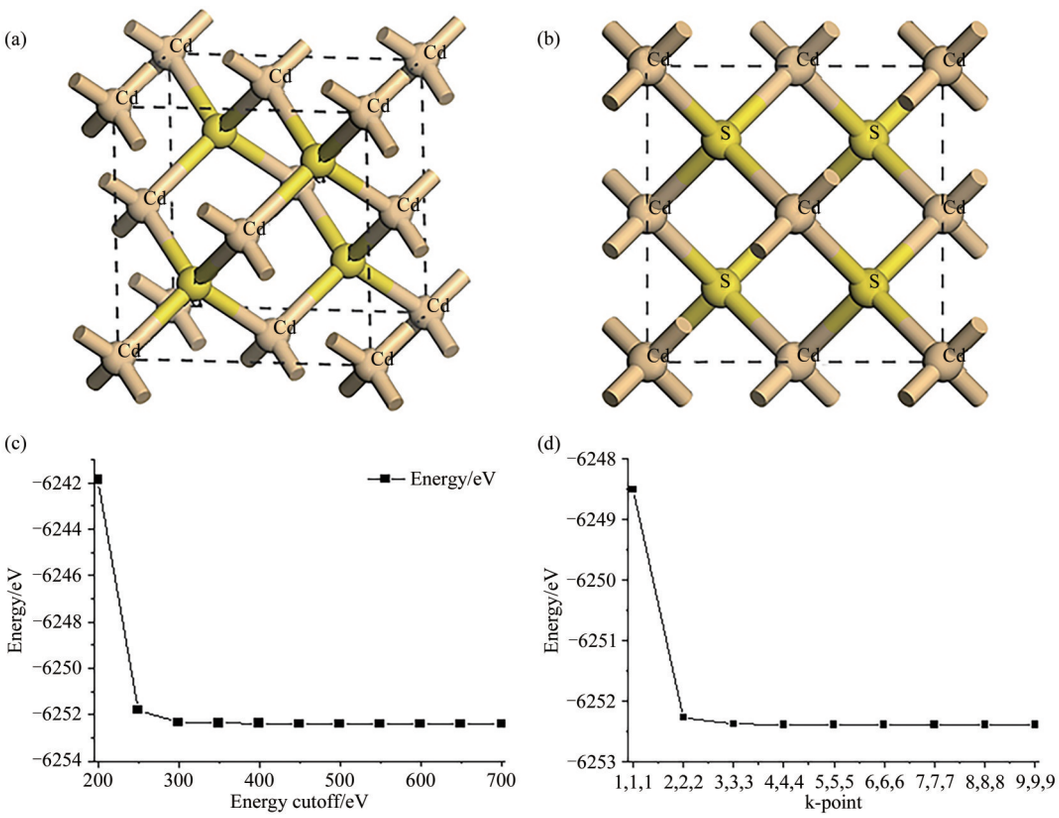


(a) Calculation model for standard structure of CdS; (b) Calculation model for geometry optimized structure CdS; (c) Selected cutoff energy; (d) K-point test

Fig. 1 Schematic illustration for the calculation model of CdS and calculation parameters

图 1 CdS的计算模型示意图和计算参数

## 2 Results and discussion

### 2.1 Phase structures

The phase constitution and crystalline form of the sample were measured by XRD, and the related diffraction peaks are given in Fig. 2. The pure carbon cloth (CC) shows a broad peak at 26° relevant to the (002) crystal plane of the carbon fiber[37]. For CC/$AgVO_3$, only the diffraction peaks of $AgVO_3$ (JCPDS card No. 29-1154) can be observed and the peak relating to carbon cloth is unobservable, indicating that the carbon cloth was completely covered by $AgVO_3$[38]. The diffraction peaks of CC/CdS at 24.9°, 26.66°, 28.33°, 36.82°, 43.90°, 48.12° and 52.11° correspond to (100), (002), (101), (102), (110), (103), and (112) lattice planes of CdS (JCPDS card No. 80-0006), respectively[39]. Meanwhile, a weak diffraction peak at 26° corresponding to carbon cloth is detected due to the partial exposure of the carbon fibers uncovered by the CdS. The CC/P-CdS exhibits similar diffraction peaks as that of CC/CdS without the detection of $AgVO_3$, illustrating the dissolution of $AgVO_3$ template during the hydrothermal process. Moreover, the peak intensity of CdS in CC/P-CdS is

stronger than that of CC/CdS, reflecting a higher crystallization of CdS in CC/P-CdS.

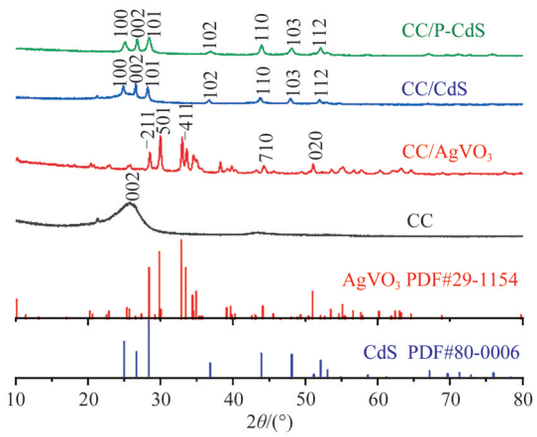


Fig. 2　XRD patterns of CC, CC/$AgVO_3$, CC/CdS and CC/P-CdS

图 2　CC、CC/$AgVO_3$、CC/CdS 和 CC/P-CdS 的 XRD 图

## 2.2　Morphology

The morphologies of pure carbon cloth (CC), CC/$AgVO_3$, CC/CdS and CC/P-CdS are shown in Fig. 3. The CC is composed of many carbon fibers with an average diameter of 10 μm (Fig. 3(a)). The high magnification image displays relatively smooth outward appearance of the carbon fiber (Fig. 3(b)). In the case of CC/$AgVO_3$, the carbon fibers are completely covered by large amounts of crisscrossed $AgVO_3$ nanowires with diameter of about 250–500 nm (Fig. 3(c) and 3(d)). The CC/CdS also shows the fiber structure of the carbon cloth (Fig. 3(e)). However, the surface of carbon fibers becomes coarse, which has been interspersed with many agglomerated CdS nanospheres self-assembled by hexagonal nanosheets (Fig. 3(f)). As for CC/P-CdS, the $AgVO_3$ nanowires originally covering the surface of the carbon cloth have disappeared and been replaced by a dense membrane (Fig. 3(g)). Further observation from the higher magnification SEM image reveals that the membrane consists of densely packed nanorods with diameter of 350–500 nm (Fig. 3(h)), which are assembled by many polygonal CdS nanoparticles according to the XRD analysis.

The microstructure of the CdS nanorods on carbon cloth was further surveyed by transmission electron microscopy (TEM). As can be seen from Fig. 4(a), the CdS nanorod has a porous structure which is made up of many polygonal nanoparticles. Furthermore, a long crevice can be faintly seen along the axial direction of the CdS nanorod deriving from the dissolution of the $AgVO_3$ nanowire during the hydrothermal reaction. The high-resolution transmission electron microscopy (HRTEM) image (Fig. 4(b)) of the edge area of nanorod shows clear lattice fringes with interplanar crystal spacing of 0.32 nm belonging to the (101) crystallographic plane of CdS[40]. The elemental component of the nanorod was further determined by energy dispersive spectrometer (EDS), as shown in Fig. 4(c). The EDS spectrum shows that the nanorod mainly comprises Cd and S elements along with tiny amounts of Ag, V and O elements. The atomic ratio of Cd to S is close to 1∶1, indicating that the Cd species in the nanorod exist mainly in the form of CdS. The elemental mapping reveals evenly distribution of both Cd and S elements on the nanorod. All the results indicate the successful preparation of CdS nanorods, which is well consistent with the XRD analysis.

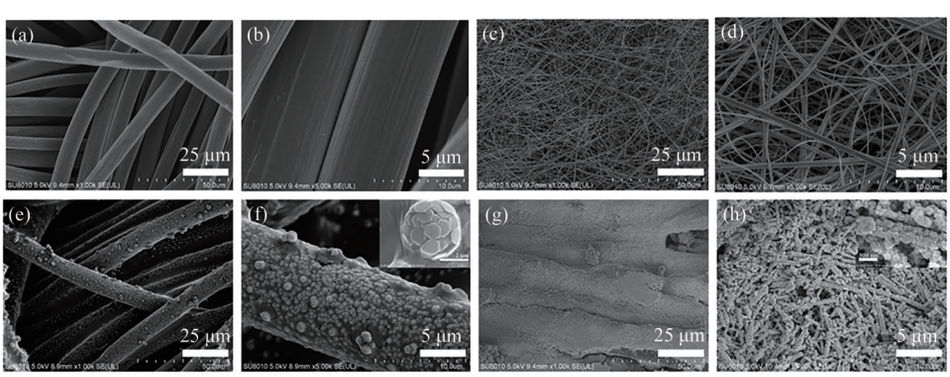


(a), (b) carbon cloth; (c), (d) CC/$AgVO_3$; (e), (f) CC/P-CdS

Fig. 3　SEM images of the as-prepared samples

图 3　所制备样品的 SEM 图像

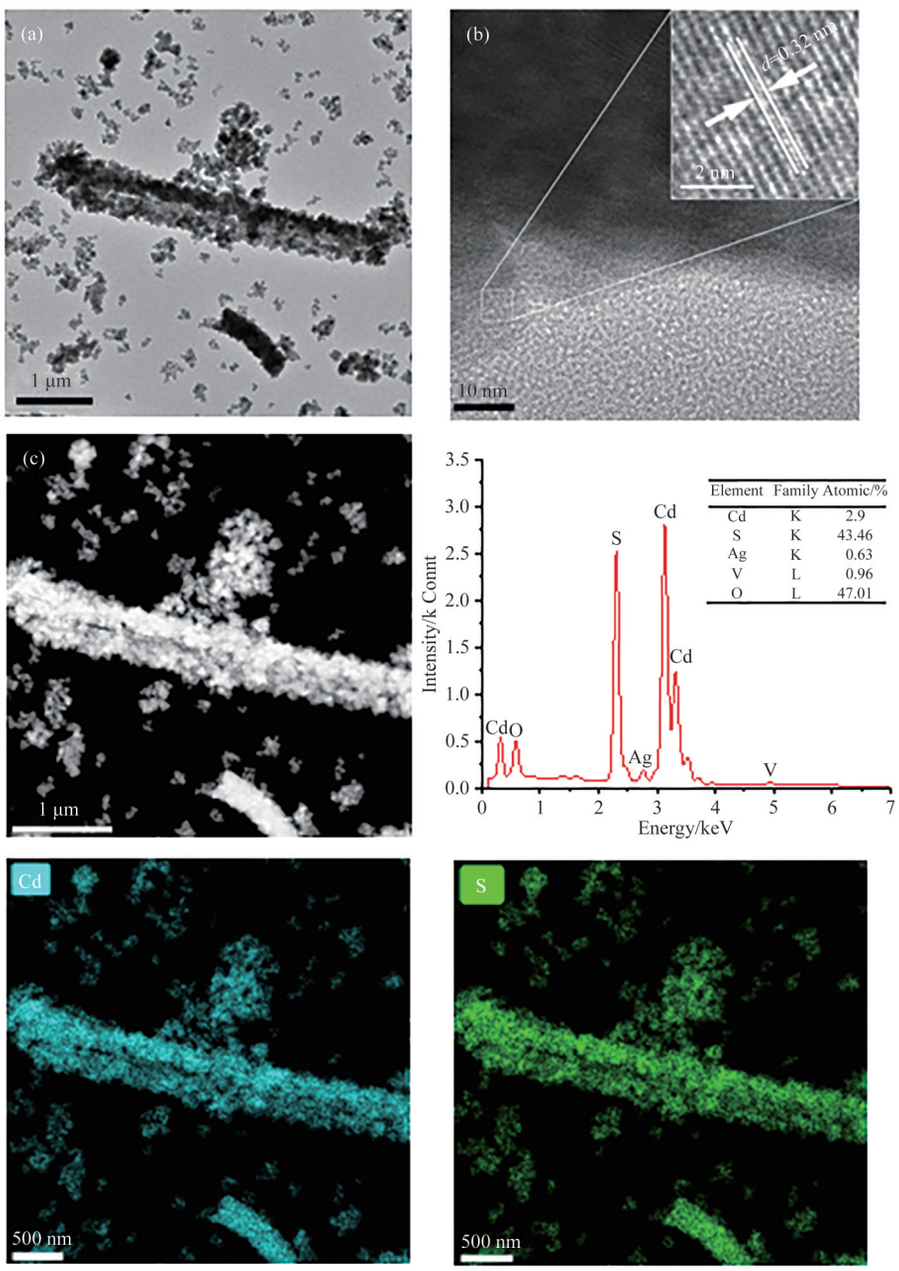


(a),(b) TEM images; (c) Elemental mappings

Fig. 4 TEM images and corresponding elemental mappings of CC/P-CdS

图4 CC/P-CdS 的TEM图像和对应的元素分布图

### 2.3 XPS analysis

The constitution and states of chemical elements on the surface of CC/P-CdS were further confirmed by XPS analysis and the obtained energy spectra are shown in Fig. 5. The XPS survey spectrum of the sample shows the presence of Cd, S, Ag and O elements (Fig. 5(a)), which agrees with the EDS analysis as described above. The peak of C 1s mainly originates from the uncovered carbon fibers. The high-resolution spectrum of Cd 3d (Fig. 5(b)) exhibits two peaks locating at 410.25 and 403.53 eV, deriving from the typical $Cd^{2+}$ of CdS in CC/P-CdS, respectively[41]. By curve fitting, the S 2p spectrum (Fig. 5(c)) can be parted into two peaks at 159.78 and 161.01 eV, which correspond to the characteristic peaks of $S^{2-}$ in CdS[42]. The XPS spectrum of Ag 3d (Fig. 5(d)) can be deconvoluted into four peaks at 366.36, 367.6, 372.35 and 373.56 eV. The two relatively strong peaks at 366.36 and 372.35 eV can be designated to the

formation of Ag—C bonds[43]. The two relatively weak peaks at 367.6 and 373.56 eV indicate the presence of $Ag_2O$[44]. It is clear from the V 2p spectrum that no peaks can be found for vanadium-related species due to the decomposition of $AgVO_3$ (Fig. 5(e)). In Fig. 5(f), the fitted XPS spectrum of O 1s shows a characteristic peak at 531.29 eV corresponding to the hydroxyl oxygen (—OH)[36], while a noticeable shoulder peak at 529.93 eV suggests the presence of Ag—O bond in $Ag_2O$[45].

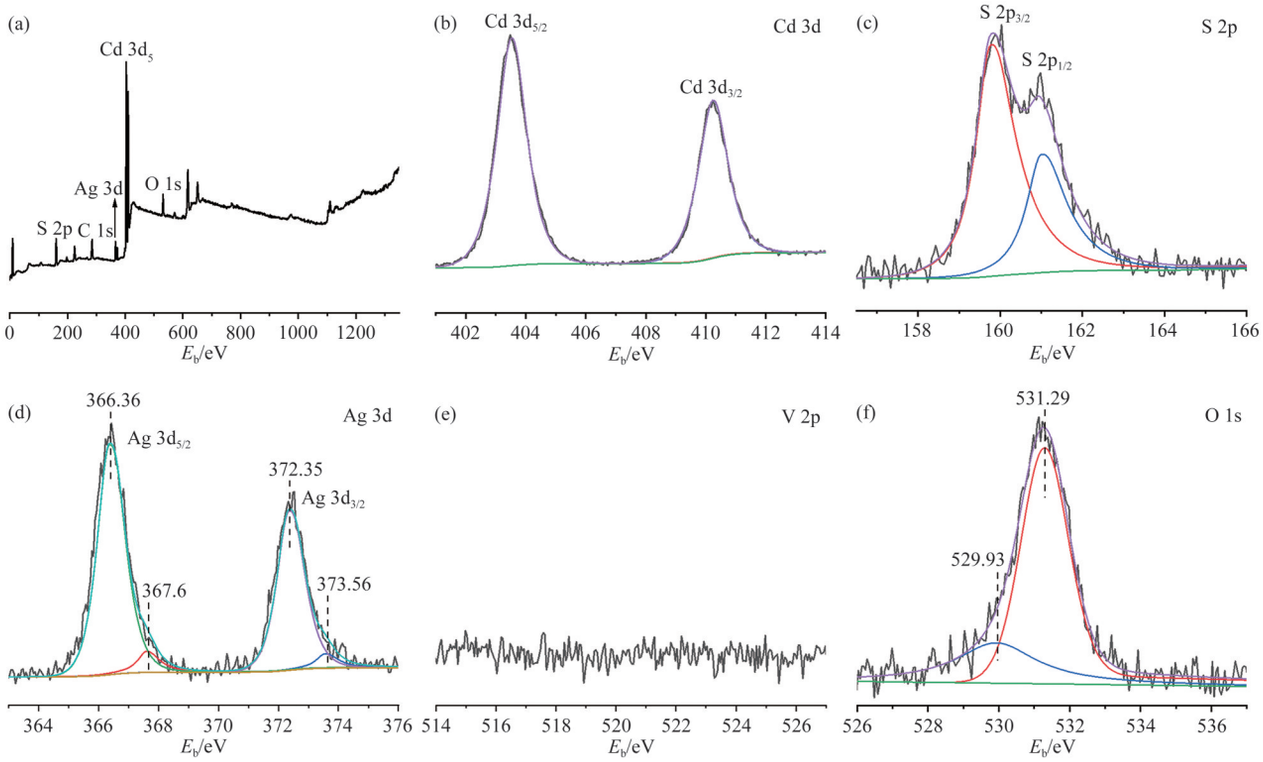


(a) Survey spectra; (b) Cd 3d; (c) S 2p; (d) Ag 3d; (e) V 2p; (f) O 1s

Fig. 5　XPS spectra of CC/P-CdS and relating elements

图 5　CC/P-CdS 及其相关元素的 XPS 谱图

## 2.4　Optical properties and theoretical calculations

The light absorption behaviors of the samples were tested by UV-vis diffuse reflectance spectroscopy (UV-DRS). As depicted in Fig. 6(a), all the samples exhibit absorption from ultraviolet light to visible light region. The dark grey carbon cloth shows a high absorption in the whole UV-visible light zone. For the CC/$AgVO_3$, a strong absorption at wavelength of approximately 550 nm was attributed to the intrinsic absorption of $AgVO_3$. The CC/CdS exhibits a relatively higher light absorption in the whole region being ascribed to the low loading of CdS on the carbon fibers (see inserted digital photos in Fig. 6(a)). As a result, many carbon fibers uncovered by the CdS contribute to the higher optical absorption. The CC/P-CdS exerts a sharp intrinsic absorption wavelength of about 600 nm. The band gap of P-CdS on carbon fibers was computed to be 2.18 eV according to the Tauc plots method, as shown in Fig. 6(b). The valence band potential ($E_{VB}$) of a semiconductor can be determined by $E_{VB} = X - E_e + 0.5\ E_g$ while the conduction band potential $E_{CB} = E_{VB} - E_g$.[46] Herein, X denotes the absolute electronegativity of the semiconductor, which has a value of 5.19 eV for CdS[47]. $E_e$ is a constant (about 4.5 eV) with respect to the standard hydrogen electrode[29]. Thus, the $E_{VB}$ and $E_{CB}$ potentials of P-CdS are 1.78 and −0.40 eV, respectively.

The electronic properties of CdS were further elucidated by calculating with DFT using materials studio, and the calculated band structure and electronic density of states (DOS) of CdS were shown in Fig. 7. Fig. 7(a) shows that the direct band gap energy of CdS calculated using HSE06 functions is 2.38 eV. Both valence-band maximum (VBM) and

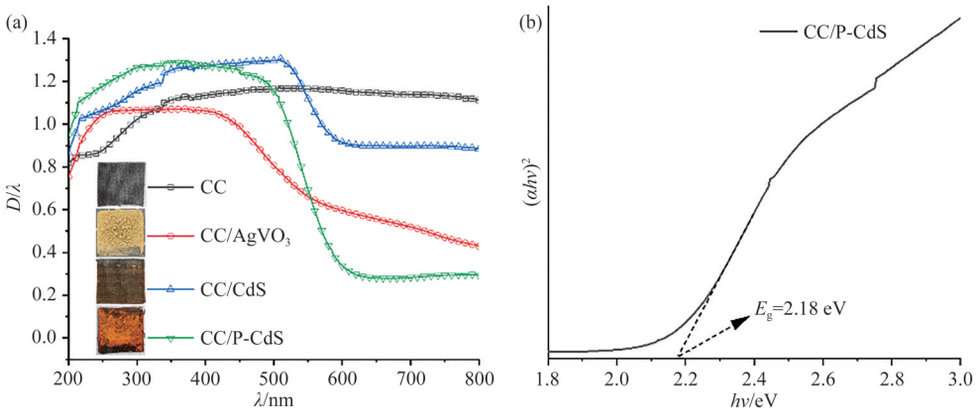


(a) UV-vis diffuse reflectance spectra of as-prepared samples; (b) Tauc-plot of porous CdS nanorods

Fig. 6 The absorption spectra of the samples and the calculated bandgap

图6 样品的吸收光谱图及其计算的禁带宽度

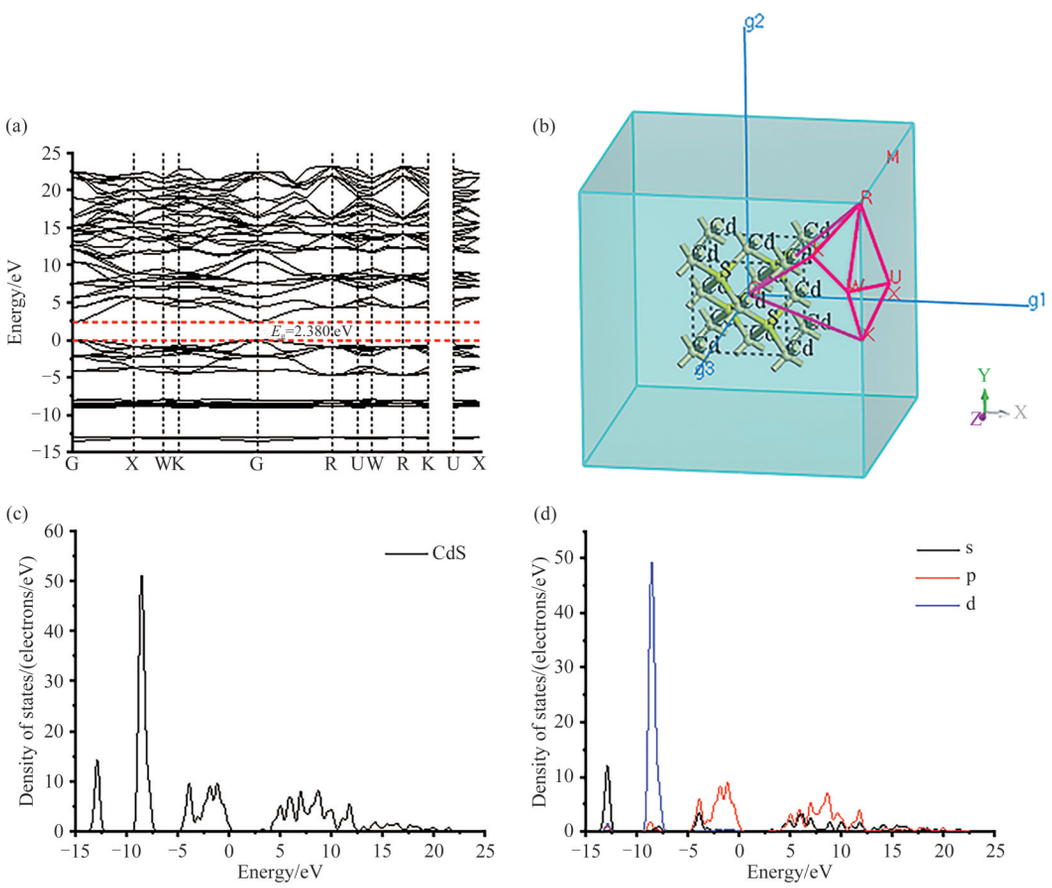


(a) Band structure of CdS; (b) K-space of CdS structure; (c) Calculated total DOS of CdS; (d) Calculated partial DOS of CdS

Fig. 7 Calculated band structure and state density information of CdS

图7 计算的CdS的能带结构图和态密度信息

conduction-band minimum (CBM) are situated in the G point. In this calculation, the band structure that represents the possible electrons propagating in crystal structures was distributed within the Brillouin zone of G-X-W-K-G-R-U-W-R-K-U-X space for the CdS structures (Fig. 7(b)).[48]. The hybrid functions not only give precise calculation results for the band gap energy but also reproduce the band edge position and electronic localization of d states well[49]. The DOS was calculated to confirm the nature of the CdS semiconductor. It can be seen from Fig. 7(c) and d that the calculated valence band of CdS mainly originates from the occupation of S 3p rather than from Cd 4d states, and the conduction band largely

originates from Cd 3p states.

### 2.5 Photocatalytic activity

The performances of the CC/P-CdS were appraised by photocatalytic reduction of the potassium dichromate in aqueous solution exposure to visible light. The photocatalyst fines were suspended in the solution and magnetically stirred in the dark for 60 min to reach adsorption saturation of potassium dichromate prior to light illumination. The concentration of Cr(Ⅵ) in the solution was determined by diphenylcarbazide spectrophotometry method. The Cr(Ⅵ) ions can react with diphenylcarbonic dihydrazine to form a purplish red complex with a characteristic absorption peak at about 540 nm. Fig. 8 shows the concentration change of Cr(Ⅵ) when reduced by CC/P-CdS. It can be clearly seen that CC/P-CdS showed a strong adsorption of Cr(Ⅵ) after being kept in the dark environment for 60 min. The content of Cr(Ⅵ) in the solution was reduced by 41% when an adsorption-desorption equilibrium was reached. The peak intensity at 540 nm gradually decreased with increasing illumination time, indicating that the concentration of Cr(Ⅵ) in the solution gradually reduced. After 40 min of illumination, the concentration of Cr(Ⅵ) is only 1.9% of the concentration at the beginning of the illumination.

The photocatalytic activities of the samples were compared in Fig. 9(a) and 9(b). It can be seen from

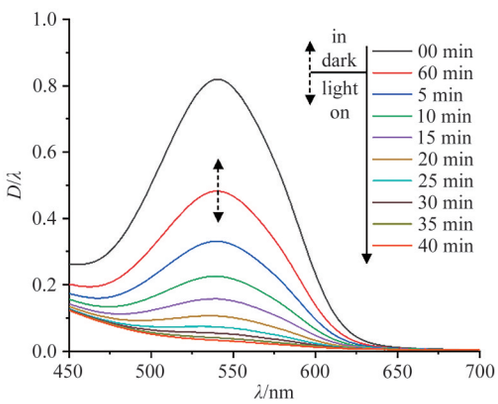


Fig. 8　Absorption changes of Cr(Ⅵ) by diphenylcarbazide spectrophotometry method in the presence of CC/P-CdS

图 8　通过二苯碳酰二肼分光光度法测得 Cr(Ⅵ)在 CC/P-CdS 作用下的吸收变化曲线图

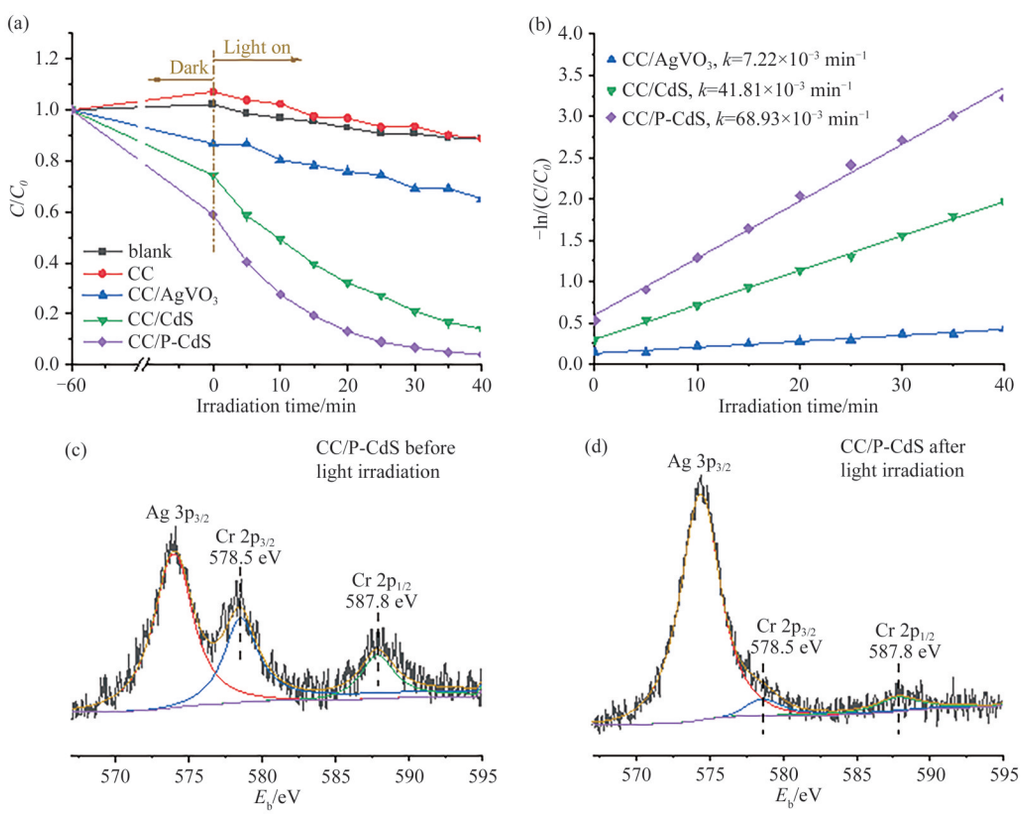


(a) Hotocatalytic activity; (b) Reaction rate constants; (c) High-resolution XPS spectra of Cr 2p before photocatalytic reaction; (d) High-resolution XPS spectra of Cr 2p after photocatalytic reaction

Fig. 9　Comparison of the photocatalytic activity of the samples and high-resolution XPS spectra of Cr 2p

图 9　样品的光催化活性比较以及 Cr 2p 的 XPS 高分辨谱图

Fig. 9(a) that the concentration of Cr(Ⅵ) in the blank sample (pure solution without the addition of photocatalysts) shows no obvious change in the adsorption process. Cr(Ⅵ) in the presence of pure carbon cloth (CC) is no exception. About 13% and 26% of Cr(Ⅵ) ions were respectively adsorbed by CC/$AgVO_3$ and CC/CdS after reaching adsorption-desorption equilibrium. The adsorption ratio of Cr(Ⅵ) ions on the CC/P-CdS in the dark reached as high as 41%, mainly because of the larger specific surface area of porous CdS nanorods. After 40 mins of visible-light exposure, 25 % of Cr(Ⅵ) were reduced by CC/$AgVO_3$, while the reduction ratios of Cr(Ⅵ) to Cr(Ⅲ) by CC/CdS and CC/P-CdS were 91.8 % and 98.1 %, respectively. The reaction rate constant of CC/P-CdS ($68.93 \times 10^{-3}$ $min^{-1}$) exceeded that of CC/$AgVO_3$ ($7.22 \times 10^{-3}$ $min^{-1}$) and CC/CdS ($41.81 \times 10^{-3}$ $min^{-1}$) by a factor of 9.55 and 1.65 times, as shown in Fig. 9(b).

In consideration of the high adsorption capacity of CC/P-CdS for Cr(Ⅵ) ions, the high-resolution XPS spectra of Cr ions adsorbed on the CC/P-CdS before light illumination and after light irradiation for 40 min were carried out respectively to fully illustrate the reduction of Cr(Ⅵ) to Cr(Ⅲ) by CC/P-CdS. As can be seen from Fig. 9(c), the XPS spectrum of Cr 2p can be deconvoluted into two peaks locating at 578.5 and 587.8 eV, which correspond to the Cr(Ⅵ) that originated from the potassium dichromate adsorbed by the CC/P-CdS [9]. After light irradiation for 40 min, the XPS peak intensity of Cr $2p_{3/2}$ and Cr $2p_{1/2}$ significantly decreased, as shown in Fig. 9(d). This can be ascribed to the truth that the Cr(Ⅵ) ions absorbed on the surface of CC/P-CdS had been largely reduced to Cr(Ⅲ), which desorbed from the CC/P-CdS and transferred to the solution system in quick succession. It also explains why no XPS peaks corresponding to Cr(Ⅲ) can be found on the surface of CC/P-CdS after light irradiation. Moreover, the reduction ratio of Cr(Ⅵ) to Cr(Ⅲ) in the presence of CC/P-CdS still reached 92% after the fourth cycle (Fig. 10), exhibiting good recyclability and photocatalytic stability.

The schematic of mechanism for reduction of potassium dichromate by CC/P-CdS is shown in Fig. 11.

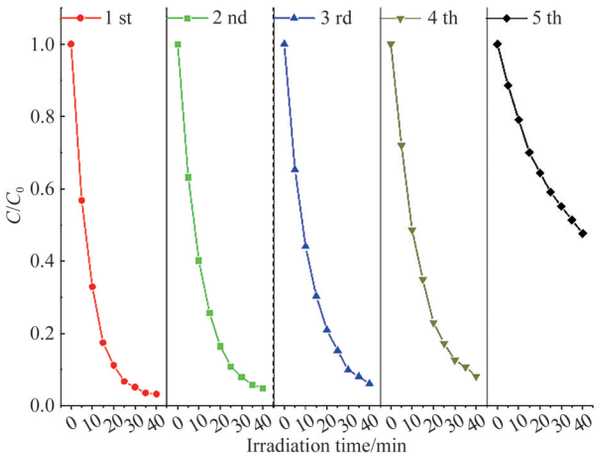


Fig. 10 Photocatalytic recyclability of the CC/P-CdS for Cr(Ⅵ) reduction under visible light irradiation

图 10 CC/P-CdS在可见光照射下还原Cr(Ⅵ)的光催化循环稳定性测试

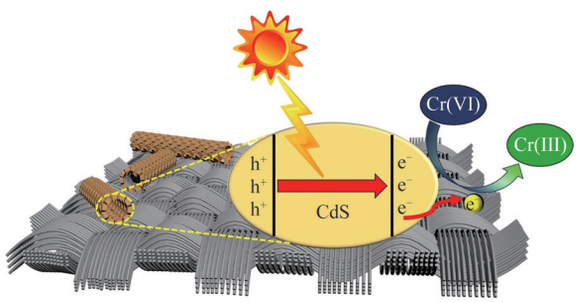


Fig. 11 Proposed mechanism for the carbon cloth-supported porous CdS nanorods as photocatalyst in Cr(Ⅵ) reduction

图 11 碳布负载多孔CdS纳米棒在Cr(Ⅵ)还原中的光催化作用机理

CdS has an isoelectric point of 5.5[50], which is positively charged in acidic potassium dichromate solution. Thus, more $Cr_2O_7^{2-}$ ions can be adsorbed by the porous CdS nanorods. When irradiated with visible light, the CdS was excited and electrons generated in the valence band (VB) leaped to the conduction band (CB), resulting in the generation of holes in the valence band (VB). The $E_{CB}$ of CdS is −0.305 eV (relative to NHE), while the potential of Cr(Ⅵ)/$Cr^{3+}$ is 0.121 eV (relative to NHE)[51]. Hence, the Cr(Ⅵ) ions adsorbed on the surface of porous CdS nanorods can be reduced to Cr (Ⅲ) by photogenerated electrons in the conduction band. In addition, carbon fiber cloth has excellent electrical conductivity and can quickly receive the photogenerated electrons from CdS, which promotes the separation of electron-hole pairs. Furthermore, CC/P-CdS cloth possesses good reusability in the practical application for reducing various heavy metal ions.

## 3 Conclusions

In summary, porous CdS nanorods were successfully synthesized on carbon fiber cloth substrate by a simple two-step hydrothermal method using $AgVO_3$ nanowires as templates. The porous CdS nanorods not only provided larger specific surface area for Cr(Ⅵ) ions absorption, but also exposed more active sites for photocatalytic reduction of Cr(Ⅵ) ions. The adsorption ratio of Cr(Ⅵ) ions onto the carbon cloth-supported porous CdS nanorods in the dark reached as high as 41%, and 98.1% of Cr(Ⅵ) ions had been reduced to Cr(Ⅲ) within 40 min of visible light irradiation. XPS analysis also confirmed the fully reduction of Cr(Ⅵ) ions adsorbed on the carbon cloth-supported porous CdS nanorods. The excellent conductivity of carbon fibers facilitated effectively separation between electrons and holes, which was also responsible for the high photocatalytic reduction activity of porous CdS nanorods. Meanwhile, the carbon cloth-supported porous CdS nanorods can be easily removed from the contaminant solution and be reutilized. This study provides an environmentally friendly method for fabrication of immobilized photocatalysts with high activity in the practical application of reducing heavy metal ions from wastewater.

### References


[1] 李宇涵, 张敏, 谷苗莉, 等. 氧空位 $TiO_2$ 高效光催化甲醛及其反应路径[J]. 科学通报, 2020, 65(8): 718-728.

[2] GOLDER A K, CHANDA A K, SAMANTA A N, et al. Removal of hexavalent chromium by electrochemical reduction-precipitation: Investigation of process performance and reaction stoichiometry [J]. Separation and Purification Technology, 2011, 76(3): 345-350.

[3] MA H L, ZHANG Y, HU Q H, et al. Chemical reduction and removal of Cr(vi) from acidic aqueous solution by ethylenediamine-reduced graphene oxide [J]. Journal of Materials Chemistry, 2012, 22(13): 5914-5916.

[4] JEON M S, LEE TKYU, HYUNG KIM D, et al. The enhancement of redox reactions with mixed oxide catalysts by the sol-gel process[J]. Solar Energy Materials and Solar Cells, 1999, 57(3): 217-227.

[5] GAO X, JIAN S, WANG W, et al. Study on photochemical properties of a Sr-$SnS_2$/$CaIn_2S_4$ heterostructure to improve Cr(Ⅵ) removal[J]. Langmuir, 2023, 39(30): 10542-10552.

[6] SHENG S, SONG S, HU B, et al. Photocatalytic reduction of Cr(Ⅵ) using newly synthesized black phosphorus/ZnO nanocomposites [J]. Environmental Technology, 2023: 1-9.

[7] ZHANG H, LUO Y H, CHEN F Y, et al. Enhancing the spatial separation of photogenerated charges on Fe-based MOFs via structural regulation for highly-efficient photocatalytic Cr(Ⅵ) reduction[J]. Journal of Hazardous Materials, 2023, 441: 129875.

[8] CAO S, DU M, LI Y, et al. Nanosized carbonate-doped $TiO_{2-x}$ mesocrystals for visible-light-driven photocatalytic removal of water pollutants [J]. ACS Applied Nano Materials, 2020, 3(5): 4197-4208.

[9] SRIRATTANAPIBUL S, TANG I M, THONGMEE S. Photo catalytic reduction of $Cr^{6+}$ by ZnO decorated on reduced graphene oxide (rGO) nanocomposites [J]. Materials Research Bulletin, 2019, 122(1): 110705.

[10] YAN C, DONG X, WANG Y, et al. Porous $Cd_3(C_3N_3S_3)_2$/CdS composites with outstanding Cr(Ⅵ) photoreduction performance under visible light irradiation [J]. Separation and Purification Technology, 2022, 293: 121077.

[11] HU D, XU Y, ZHANG S, et al. Fabrication of redox-mediator-free Z-scheme CdS/$NiCo_2O_4$ photocatalysts with enhanced visible-light driven photocatalytic activity in Cr (Ⅵ) reduction and antibiotics degradation [J]. Colloids and Surfaces A Physicochemical and Engineering Aspects, 2021, 608: 125582.

[12] EDDY D R, PERMANA M D, SAKTI L K, et al. Comparative studies of synthesis of Ag/$Ag_2O$ nanoparticles by sol-gel and sonochemical method as removal of Cr(Ⅵ)[J]. Emergent Materials, 2023, 6(4): 1231-1242.

[13] WAN Z, MAO Q, XIANG J, et al. Greatly increased visible-light photocatalytic activity of $SnS_2$/carbon nanotube composite for Cr(Ⅵ) reduction: Insights into effects of solid acid structure [J]. Journal of Materials Science & Technology, 2023, 161: 233-244

[14] YU F, CEN L, LEI C, et al. Fabrication of recyclable UiO-66-$NH_2$/PVDF hybrid fibrous membrane for Cr(Ⅵ) removal in wastewater [J]. Journal of Industrial and Engineering Chemistry, 2023, 123: 104-115.

[15] 李雨涵, 谷苗莉, 欧阳平, 等. 锡酸锌光催化剂的制备及表面改性策略研究进展[J]. 功能材料, 2022, 53(11): 11075-11080.

[16] 陈邦富, 欧阳平, 李雨涵, 等. $ZnSn(OH)_6$ 基纳米材料

在环境光催化中的应用[J]. 化工进展, 2023, 42(2): 756-764.

[17] DENG L, LI Y, ZHANG Z, et al. In situ growth of ultrathin CdS nanosheets on porous carbon aerogels for improved photocatalytic $H_2$ production[J]. ACS Applied Nano Materials, 2023, 6(17): 16009-16015.

[18] LI X, WANG J, WANG H, et al. CoP-embedded graphitic N-doped C nanosheets in ohmic contact with S-deficient CdS nanocrystals triggering efficient visible-light photocatalytic $H_2$ evolution [J]. ACS Applied Nano Materials, 2023, 6(6): 4437-4448.

[19] REN Y, DONG T, DING S, et al. AgBr nanoparticles anchored on CdS nanorods as photocatalysts for $H_2$ evolution [J]. ACS Applied Nano Materials, 2021, 4(9): 9274-9282.

[20] CHAI Z M, WANG B H, TAN Y X, et al. Enhanced photocatalytic activity for selective oxidation of toluene over cubic-hexagonal CdS phase junctions[J]. Industrial & Engineering Chemistry Research, 2021, 60(30): 11106-11116.

[21] WEI C, ZANG W, YIN J, et al. Biomolecule-assisted construction of cadmium sulfide hollow spheres with structure-dependent photocatalytic activity [J]. Chemphyschem, 2013, 14(3): 591-596.

[22] YANG Y, YANG K, WANG J, et al. Fabrication and characterization of CdS nanowires templated in tobacco mosaic virus with improved photocatalytic ability [J]. Applied Microbiology and Biotechnology, 2021, 105(21-22): 8255-8264.

[23] CHEN F, ZHOU R, YANG L, et al. One-step fabrication of CdS nanorod arrays via solution chemistry [J]. The Journal of Physical Chemistry C, 2008, 112(35): 13457-13462.

[24] LIU C, LI J, SUN L, et al. Visible-light driven photocatalyst of CdTe/CdS homologous heterojunction on N-rGO photocatalyst for efficient degradation of 2, 4-dichlorophenol [J]. Journal of the Taiwan Institute of Chemical Engineers, 2018, 93: 603-615

[25] SERRÀ A, PIP P, GÓMEZ E, et al. Efficient magnetic hybrid ZnO-based photocatalysts for visible-light-driven removal of toxic cyanobacteria blooms and cyanotoxins[J]. Applied Catalysis B: Environmental, 2020, 268: 118745.

[26] 张敏, 陈邦富, 李雨涵, 等. 微波法制备光催化纳米材料的应用及其性能研究[J]. 功能材料, 2022, 53(11): 11081-11087.

[27] 虞梦雪, 常世鑫, 李覃, 等. 天然矿物光催化对环境的影响[J]. 中南民族大学学报(自然科学版), 2024, 43(2): 156-165.

[28] ZHANG Y, LUO L, SHI Z, et al. Synthesis of $MoS_2$/CdS heterostructures on carbon-fiber cloth as filter-membrane-shaped photocatalyst for purifying the flowing wastewater under visible-light illumination [J]. ChemCatChem, 2019, 11(12): 2855-2863.

[29] ZHU K, WANG S, LIU H, et al. Heteroatom-doped porous carbon nanoparticle-decorated carbon cloth (HPCN/CC) as efficient anode electrode for microbial fuel cells (MFCs) [J]. Journal of Cleaner Production, 2022, 336: 130374.

[30] CHEN W, WEI T, MO L E, et al. $CoS_2$ nanosheets on carbon cloth for flexible all-solid-state supercapacitors[J]. Chemical Engineering Journal, 2020, 400: 125856.

[31] CHEN Q, CHEN S, ZHAO L, et al. Interface coating of iron nitride on carbon cloth for reversible lithium redox in rechargeable battery [J]. Chemical Engineering Journal, 2022, 431: 133961.

[32] LIU Y, WANG W, SI M, et al. Carbon cloth-supported $MoS_2$/$Ag_2S$/$Ag_3PO_4$ composite with high photocatalytic activity and recyclability [J]. ChemCatChem, 2019, 11(3): 1017-1025.

[33] 常世鑫, 虞梦雪, 俞迨, 等. 石墨相氮化碳光催化还原$CO_2$研究进展[J]. 中南民族大学学报(自然科学版), 2023, 42(6): 721-732.

[34] 李宇涵, 任字藤, 段有雨, 等. 锡酸锌基光催化材料研究进展[J]. 稀有金属, 2023, 47(1): 73-89.

[35] 陈邦富, 欧阳平, 李雨涵, 等. 羟基锡酸锌作为光催化剂的研究进展[J]. 功能材料, 2022, 11(53): 11104-11110.

[36] WU H, QIU T, ZHAO G, et al. Investigations on the reverse cationic flotation separation of quartz from hematite using polyaspartic acid as depressant [J]. Applied Surface Science, 2023, 614: 156143.

[37] ZHANG Y, SUN A, XIONG M, et al. $TiO_2$/BiOI p-n junction-decorated carbon fibers as weavable photocatalyst with UV-vis photoresponsive for efficiently degrading various pollutants [J]. Chemical Engineering Journal, 2021, 415: 129019.

[38] ZHANG X, ZHANG J, YU J, et al. Fabrication of $InVO_4$/$AgVO_3$ heterojunctions with enhanced photocatalytic antifouling efficiency under visible-light [J]. Applied Catalysis B: Environmental, 2018, 220: 57-66.

[39] TAYYAB M, LIU Y, MIN S, et al. Simultaneous hydrogen production with the selective oxidation of benzyl alcohol to benzaldehyde by a noble-metal-free photocatalyst VC/CdS nanowires[J]. Chinese Journal of Catalysis, 2022, 43(4): 1165-1175.

[40] SHEN X, ZHANG Y, SHI Z, et al. Construction of

$C_3N_4$/CdS nanojunctions on carbon fiber cloth as a filter-membrane-shaped photocatalyst for degrading flowing wastewater [J]. Journal of Alloys and Compounds, 2021, 851: 156743.

[41] ZHOU M, WANG S, YANG P, et al. Boron carbon nitride semiconductors decorated with CdS nanoparticles for photocatalytic reduction of $CO_2$ [J]. ACS Catalysis, 2018, 8(6): 4928-4936.

[42] JIA Y, ZHANG Y, ZHANG X, et al. Novel CdS/PANI/MWCNTs photocatalysts for photocatalytic degradation of xanthate in wastewater [J]. Separation and Purification Technology, 2023, 309: 123022.

[43] BOUKHVALOV D, ZHIDKOV I, KURMAEV E, et al. Atomic and electronic structures of stable linear carbon chains on Ag-nanoparticles [J]. Carbon, 2018, 128: 296-301.

[44] DE A K, MAJUMDAR S, PAL S, et al. Zn doping induced band gap widening of $Ag_2O$ nanoparticles [J]. Journal of Alloys and Compounds, 2020, 832: 154127.

[45] YADAV S, MITTAL A, SHARMA S, et al. Highly efficient $Ag_2O$ loaded ZnO/$Al_2O_3$ coupled catalyst and its photocatalytic application [J]. Inorganic Chemistry Communications, 2021, 130: 108738.

[46] ZHANG Y, SHI Z, LUO L, et al. Construction of titanium dioxide/cadmium sulfide heterojunction on carbon fibers as weavable photocatalyst for eliminating various contaminants [J]. Journal of Colloid and Interface Science, 2020, 561: 307-317.

[47] JIA X, TAHIR M, PAN L, et al. Direct Z-scheme composite of CdS and oxygen-defected $CdWO_4$: An efficient visible-light-driven photocatalyst for hydrogen evolution [J]. Applied Catalysis B: Environmental, 2016, 198: 154-161.

[48] SETYAWAN W, CURTAROLO S. High-throughput electronic band structure calculations: Challenges and tools [J]. Computational Materials Science, 2010, 49(2): 299-312.

[49] SINAR MASHURI S I, KASIM M F, MOHD KAUS N H, et al. Photo-response range extension of Z-scheme ZnO/CdS for LED-light-driven photo-active catalyst [J]. Renewable and Sustainable Energy Reviews, 2023, 184: 113602.

[50] TAŞCıOĞLU S, TAŞ D. Surfactant effect on determination of $Cu^{2+}$ and $Cd^{2+}$ ions by ion-selective electrodes providing evidence for the discrepancy between the point of zero charge and the isoelectric point of CdS [J]. Colloids and Surfaces A: Physicochemical and Engineering Aspects, 2007, 302(1/3): 349-353.

[51] WANG L, KARUTURI S K, ZAN L. $SnS_2$-$In_2S_3$ p-n heterostructures with enhanced $Cr^{6+}$ reduction under visible-light irradiation [J]. Applied Surface Science, 2021, 537: 148063.

(责编&校对　刘钊)